Nanoscale

PAPER

View Article Online
View Journal | View Issue

Cite this: *Nanoscale*, 2023, **15**, 11107

Surface–particle interactions control the escape time of a particle from a nanopore-gated nanocavity system: a coarse grained simulation†

Robert Zando, [a] Mauro Chinappi,[b] Cristiano Giordani,[c,d] Fabio Cecconi [e] and Zhen Zhang [a]

Nanopores and nanocavities are promising single molecule tools for investigating the behavior of individual molecules within confined spaces. For single molecule analysis, the total duration of time the analyte remains within the pore/cavity is highly important. However, this dwell time is ruled by a complex interplay among particle–surface interactions, external forces on the particle and Brownian diffusion, making the prediction of the dwell time challenging. Here, we show how the dwell time of an analyte in a nanocavity that is connected to the external environment by two nanopore gates depends on the sizes of the nanocavity/nanopore, as well as particle–wall interactions. For this purpose, we used a coarse-grained model that allowed us to simulate hundreds of individual analyte trajectories within a nanocavity volume. We found that by increasing the attraction between the particle and the wall, the diffusion process transforms from a usual 3D scenario (repulsive wall) to a 2D motion along the cavity surface (highly attractive wall). This results in a significant reduction of the average dwell time. Additionally, the comparison of our results with existing theories on narrow escape problem allowed us to quantify the reliability of theory derived for ideal conditions to geometries more similar to actual devices.

Received 22nd March 2023,
Accepted 8th June 2023

DOI: 10.1039/d3nr01329d

rsc.li/nanoscale

1 Introduction

The motion of single nanoentities in confined geometries is relevant to a wide number of biological processes. Among others,[1] examples include the diffusion of molecules on a crowded membrane[2] and the modelling of synaptic currents.[3] A common feature of all these scenarios is that a single particle diffuses in a confined environment until it reaches a specific location. This location can be a site where the molecules interact with a specific ligand or an aperture on the surface of the confining space. In literature, this class of problems has traditionally been referred to as the Narrow Escape Problem (NEP), and is centered on calculating the mean first passage time of a diffusion process of a particle to a target much smaller than the size of the confining space.[4–8]

NEP's for a single molecule are also highly relevant to the study of the behavior of single molecules in sensing devices, such as nanopores[9–15] or nanocavities,[16–18] since, once the analyte has been drawn into the confining geometry through external forces such as electrophoresis[19,20] or dielectrophoresis[21,22] it needs to remain within long enough to allow the acquisition of a signal from it. It is, therefore, crucial to investigate which factors affect the dwell time of the molecules in the confining geometry.

In this study, we focus on the exit of a particle from a nanocavity that is connected to external reservoirs by two nanopores (see Fig. 1). This set-up resembles a number of solid-state nanopore systems used for sensing purposes.[9,10,23] These solid-state pores may take on a wide variety of different geometries,[24] such as cylindrical, conical or hourglass-shaped[25] (though our study focuses primarily on a cylindrical geometry configuration). The nanopore apertures on either entrance of the nanocavity may be varied in size (compared to the cavity dimensions) through the use of secondary barriers[9] or the deposition of surface additives such as carbon to reduce the opening diameter.[26,27]

In order to ensure a reasonable computational cost for our study, we made use of a "coarse-grained" approach, as commonly employed in the literature to make affordable the simu-

[a]*Division of Solid-State Electronics, Department of Electrical Engineering, Uppsala University, SE-751 03 Uppsala, Sweden. E-mail: zhen.zhang@angstrom.uu.se*
[b]*Dipartimento di Ingegneria Industriale, Università di Roma Tor Vergata, Via del Politecnico 1, Roma, Italy. E-mail: mauro.chinappi@uniroma2.it*
[c]*Grupo Productos Naturales Marinos, Facultad de Ciencias Farmacéuticas y Alimentarias, Universidad de Antioquia, Calle 70 No. 52-21, Medellín 050010, Colombia*
[d]*Instituto de Física, Universidad de Antioquia, Calle 70 No. 52-21, Medellín 050010, Colombia*
[e]*Istituto Sistemi Complessi, CNR, Via dei Taurini, Roma, Italy*
† Electronic supplementary information (ESI) available. See DOI: https://doi.org/10.1039/d3nr01329d

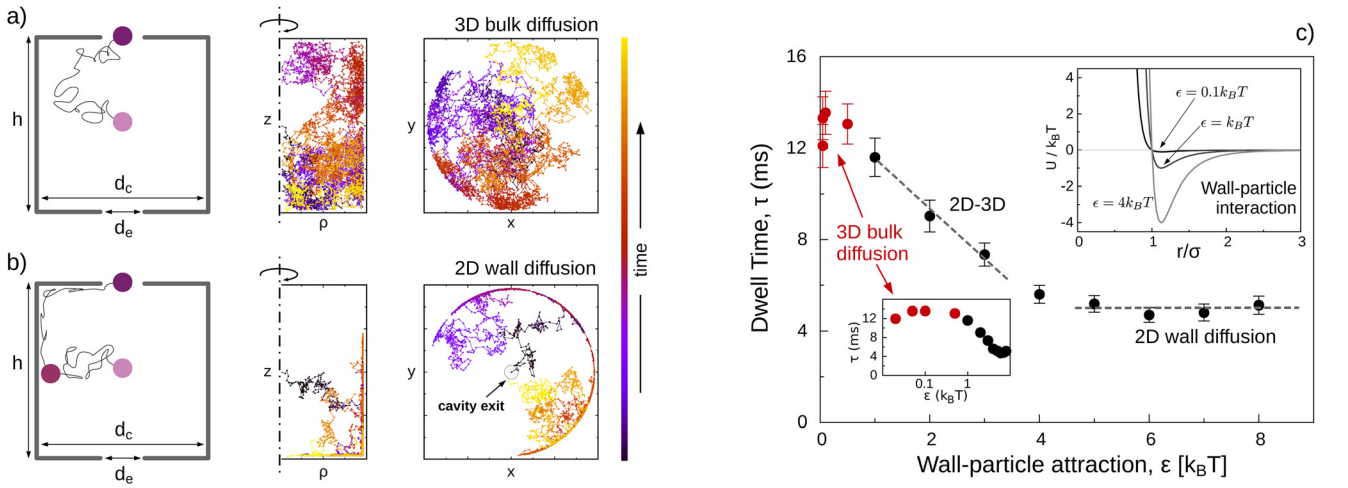

Fig. 1 Escape from a cylindrical cavity, bulk *vs.* surface diffusion. (a) When the wall particle interaction is repulsive, the particle, initially placed in the center of the cavity, diffuses in the volume until it reaches one of the two exits. This trajectory used the following conditions: ε = 0.1k_BT, d_c = 400 nm and d_e = 50 nm. The center panel is a polar representation of the trajectory, z is the axis of the cylinder, and ρ the distance between the particle an the axis. Left panel is a top view (projection on the O_{xy} plane). (b) For highly attractive particle–wall interaction, as soon as the particle hits the wall, it starts a surface diffusion along it until it reaches one of the two exits. The trajectory conditions are: ε = 6k_BT, d_c = 400 nm and d_e = 50 nm. (c) Average dwell time τ as a function of ε. The upper inset reports a sketch of the Lennard-Jones potential used to model wall–particle interaction, eqn (2), the three curves corresponding to ε = 0.1, 1, 4k_BT. The lower inset reports the same data where the logarithmic scale is used for ε/k_BT to highlight the repulsive plateau at $\varepsilon/k_BT \ll 1$ (red points).

lation of system that would be untractable by atomistic models.[9,28–30] We simulate several hundred instances of trajectories for an individual analyte particle dwelling within a nanocavity, allowing us to estimate how the average dwell time was affected by particle–surface interactions and aperture size, with a focus on two specific categories of interaction conditions. In the first, the particle–surface interaction is mainly repulsive, and the particle diffuses in the bulk of the nanocavity until it reaches one of the two exits. In the second, there is a strong attraction between the particle and the wall, where contact between the particle and the nanocavity surface confines the analyte to the wall, causing the analyte to undergo surface diffusion.

2 Model and method

The system is simulated using a Brownian model. In such methodology, molecular systems with complex structures (such as DNA or proteins) may instead by simplified to pseudo-particles that may correspond to the entire molecule, as in the case of globular proteins[31] or to monomers.[9,11,32] In our work the analyte will be modeled as a Brownian particle of given hydrodynamic diameter d_p confined by the nanocavity wall. We will also consider the possibility that the particle mobility is reduced close to the wall. Details of the methods are reported in the next sections.

2.1 Brownian model

The molecule's motion within the nanocavity is modeled through the use of the overdamped Langevin equation,[33–36]

$$\dot{\mathbf{x}} = \mu\mathbf{F}(\mathbf{x}, t) + g\boldsymbol{\zeta}(t) \quad (1)$$

where $\mathbf{x}$ represents the position of the center of the molecule, μ represents its mobility within the medium, $\mathbf{F}(\mathbf{x}, t)$ represents external deterministic forces applied to the particle including the interaction with the wall, but may also incorporate the effects of other external forces, such as those which might result from an electric field.[9,30] The noise term $g\boldsymbol{\zeta}(t)$, with $g = \sqrt{2\mu k_B T}$ representing the amplitude of the white noise $\boldsymbol{\zeta}(t)$, where k_B representing the Boltzmann constant, T representing the system temperature and μ the mobility. Reducing the particle motion to tracking its center of mass can be considered a model for globular biomolecules without large internal flexibility (*e.g.* insulin, ribonuclease, hemoglobin) and small nanoparticles.[37] The overdamped Langevin model, eqn (1), is a reasonable approximation for the transport of spheroidal particles in micro and nanofluidics[38–40] where the Reynolds number is ≪1.

2.2 Particle–wall interaction

The Lennard-Jones (LJ) potential was used to model particle–wall interaction, $\mathbf{F}$ in the Langevin eqn (1). This potential energy is determined with the equation

$$U(r) = 4\varepsilon\left[\left(\frac{\sigma_{LJ}}{r}\right)^{12} - \left(\frac{\sigma_{LJ}}{r}\right)^{6}\right] \quad (2)$$

where r is the distance between the particle and the wall (calculated as detailed in ESI Fig. S3†), ε is the potential well-depth and σ_{LJ} represents the length scale of the minimum distance between the particle center and the wall (so, in essence, the particle radius $d_p/2$). The force which results from this potential energy interaction can be expressed as the gradient of the function (*i.e.*, $\mathbf{F} = -\nabla U$). A sketch of the potential is

reported in the inset of Fig. 1c. The potential well depth ε was varied between $0.1k_BT < \varepsilon < 8k_BT$, wherein the lower bound represented a scenario in which the wall surface was highly repulsive to the analyte, and the upper bound representing a highly attractive wall.

2.3 Geometry of the nanocavity

The nanocavity is modeled as a cylinder with two apertures of equal sizes on the top and the bottom (see Fig. 1a). The analyte was presumed to have started in the center of the cylinder. There are four relevant lengths in the model: the analyte diameter (d_p), the cylinder diameter (d_c), the cylinder height (h), and the aperture diameter (d_e). The specific methods used to produce the geometry in our Brownian solver, and how this information was used to determine the wall–particle distance in eqn (2), may be found in ESI Fig. S3.†

2.4 Mobility model

Due to a variety of factors, including hydrodynamic shear and particle adsorption at the surface, the ability of the analyte to freely move within the medium is usually diminished significantly near the wall.[42–44] We considered the following expression for the mobility

$$\mu = \mu_b + \frac{\mu_w - \mu_b}{2}\left[\tanh \alpha(\sigma_\mu - r) + 1\right], \quad (3)$$

where r is the particle center to wall distance, and μ_b is the bulk mobility, for which we use the widely employed Stokes expression for a no-slip sphere $\mu_b = (3\pi d_p \eta)^{-1}$, with η the solvent viscosity. In this manuscript, we assume that the particle moves in water, so $\eta = 10^{-3}$ Pa s. eqn (3) is a sigmoid (see Results and discussion). The mobility assumes the bulk value μ_b for $r \gtrsim \sigma_\mu$ and the wall value μ_w for $r \lesssim \sigma_\mu$. The parameter α determines the steepness of the sigmoid, while σ_μ denotes the length-scale of the region where the mobility reduction due to wall–particle adhesion occurs. We set $\sigma_\mu = 1.6\left(\frac{d_p}{2}\right)$, so that when the particle adheres to the wall (due to the well of the LJ potential) it is in the low μ area adhesion region, an example of which may be found in the Results section. Concerning the numeric integration, we used the stochastic Euler algorithm[34,45] where an additional drift term $k_BT\nabla\cdot\mathbf{M}$ with $\mathbf{M}$ the mobility tensor (in our case, diagonal) is added.[46,47]

3 Results and discussion

The simulations were run using a cylindrical nanocavity with two identical apertures on its bases. The diameter of the aperture ranges from d_e = 16 nm to d_e = 100 nm while the height h, equal to its diameter of the nanocavity d_c ($h = d_c$), ranges from 200 to 400 nm. The range of potential-well depths ε is between $0.1k_BT$ (repulsive case) and $8k_BT$ (highly attracting case). A spherical particle of diameter d_p = 15 nm is initially placed in the center of the nanocavity and the simulation is stopped when the particle exits from one of the two apertures. Each data set was acquired from 200 individual trajectories, allowing us to measure the average time the particles dwells the nanocavity τ. In order to focus our analysis on the effect of the aperture size d_e and wall-confinement due to potential energy interaction, we started with homogeneous mobility, *i.e.* the particle does not experience any reduction in its mobility when it is close to the wall of the nanocavity ($\mu_w = \mu_b$ in eqn (3)).

As shown in Fig. 1a and b, one of the most notable phenomena which results from the change in potential well depth ε is an drastic alteration of the particle trajectory. For $\varepsilon \ll k_BT$ the particle undergoes a bulk 3D diffusion in the nanocavity, as seen in Fig. 1a. However, for $\varepsilon > 4k_BT$, as soon as the particle reaches a wall during its 3D diffusion, it becomes trapped at the surface and starts a 2D diffusion process along the wall, as seen in Fig. 1b. Fig. 1c reports the average dwell time τ as a function of ε for d_c = 400 nm and d_e = 50 nm, showing that the transition from the 3D bulk diffusion regime to the 2D surface diffusion scenario occurs approximately for $k_BT < \varepsilon < 4k_BT$. More specifically for $\varepsilon < k_BT$, the wall is, practically, repulsive as the thermal energy easily allows the particle to escape the LJ well (see also the inset of Fig. 1b). Instead, for $\varepsilon > 4k_BT$, the particle hardly escapes from the LJ well. As shown ESI Fig. S4,† this behavior is observed also for different aperture sizes. This transition represents a dimensional reduction in the analyte's degrees of freedom which facilitates the escape from the nanocavity because the particle performs a 2D instead of a 3D diffusion.

3.1 Comparison with theory

We compared our results against two analytical models, one for the 3D bulk diffusion and one for the 2D surface diffusion scenario. The 3D analytical prediction is taken directly (with just a slight modification) from the work of Grigoriev *et al.*,[41] providing an expression for the average escape rate from a nanocavity as a function of its volume V and the radius of the exit. More specifically, we used the following expression

$$\tau = \frac{V}{4Dd_{eff}} \quad (4)$$

where $d_{eff} = d_e - d_p$ is the effective diameter available for the analyte to exit from the nanocavity. This modification to the original Grigoriev *et al.*[41] model was necessary to account for the finite size of the particle. The other modification to the original model was to divide the average time by two since in our system there are two exits. This model assumes that the surface of the nanocavity was just a repulsive confinement. Therefore, we compared the prediction of eqn (4) for the our simulation with $\varepsilon = 0.1k_BT$ (repulsive case). Fig. 2a shows a quite strong agreement between theory and computational data.

For the surface diffusion case (attractive wall), we derived a theoretical expression for τ. In brief, as common in capture and escape problems, we used a Smoluchowski-like approach that, in absence of external forcings, amounts to calculating the flux of particles on an adsorbing boundary.[48–50] More specifically, we calculate the average time τ in which a particle that diffuses on a 2D circular crown domain bounded by an

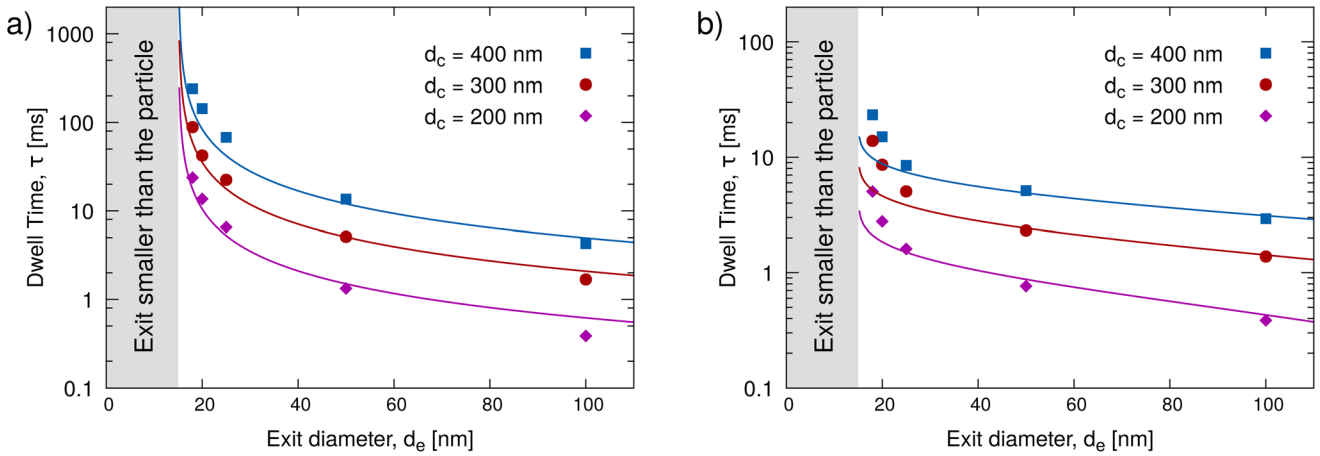

Fig. 2 Comparison with theoretical predictions. (a) Average dwell time τ as a function of the exit diameter d_e for the repulsive case ($\varepsilon = 0.1k_BT$) from our simulations (points) and from an adaptation of the results by Grigoriev *et al.*,[41] eqn (4). Three different nanocavity diameter d_c are considered. Panel (b) reports the same comparison for the attractive case ($\varepsilon = 8k_BT$). Lines refer to our 2D theoretical prediction, eqn (6). Our numerical results match the theoretical prediction for large aperture size. However, as the aperture diameter approaches the particle diameter d_p or, in other terms, since $d_{eff} = d_e - d_p$, as $d_{eff} \to 0$, the dwell time τ diverges faster than the theoretical prediction, in particular in the attractive 2D diffusion case. The grey area corresponds to $d_e < d_p$ *i.e.* exit diameter smaller that the particle diameter so that, the right boundary of the grey area corresponds to $d_{eff} = 0$. Error bars are smaller that the data point symbol sizes.

inner circle of diameter d_e, where the particles are adsorbed by an external circle of diameter d_{ext}, and where particle concentration has a prescribed value C_0 (see ESI Note S1† for details). The capture frequency $k_c = \tau^{-1}$ is given by

$$k_c = \frac{2\pi D C_0}{\ln(d_{ext}/d_e)}. \quad (5)$$

To adapt these results to our nanocavity, we need to find an estimation for d_{ext} and C_0. Concerning C_0, we considered that there is only one particle, hence, $C_0 = A^{-1}$ where A is half of the area of the nanocavity (the factor 1/2 stemming from the presence of two apertures). Concerning d_{ext}, in the simplified model that lead to eqn (5), d_{ext} is, basically, the distance from the emitting boundary and the adsorbing boundary. In our system, this would correspond to the distance from the pore exit and the first location where, the particle diffusing in the bulk, hits the wall and gets trapped. This distance, scales with the cavity size d_c, so we set $d_{ext} = d_c$. Consequently, eqn (5) reduces to

$$\tau = \frac{A}{2\pi D} \ln \frac{d_c}{d_{eff}} \quad (6)$$

where, again, we considered the effective diameter d_{eff} as the effective size of the aperture. Eqn (6) can be obtained also with other approaches, see, among others.[6–8] The predictions of this theoretical model can be seen in Fig. 2b, where they are compared against multiple data sets we simulated at $\varepsilon = 8k_BT$. Also, in this case, the computed τ demonstrated a reasonable match with analytical prediction. Deviations are observed for small apertures ($d_e < 30$ nm) suggesting that when the exit size approaches the particle size, the details of the particle–wall interaction comes into play. Ideally, these and other details can be potentially taken into account by a proper free-energy profiles in the Smoluchowski model[49,50] or including them as radiative boundary condition.[48] However, this fine tuning, even if possible, would require a detailed knowledge of the chemical interaction of a given particle with a specific nanocavity material in proximity of the aperture, a topic that is far from the general aim of this work. The overall agreement between the simulations and the theoretical predictions is also supported by a statistical analysis, as seen in ESI Table S1.†

Up to now, we showed that some trends of the dependence of the dwell time τ as a function of the geometrical features of the nanocavity can be caught by using relatively straightforward theoretical approaches. Because of this, one may ask if theoretical insights on the 2D–3D transition may be derived is similar ways. However, this case is much more complex, since in the intermediate regime ($\varepsilon = 1k_BT$ to $\varepsilon = 5k_BT$ in Fig. 1) a particle trapped in the well of the interaction potential may escape from the wall before leaving the nanocavity. Hence, the overall motion is composed by periods in which the particle diffuses in the bulk of the nanocavity and periods in which it slides along the wall. An approximated expression for the dwell time in this intermediate regime was proposed by Oshanin *et al.* (eqn (34) of ref. 6) for a spherical nanocavity. In our notation, the Oshanin result takes the form

$$\tau = \frac{\tau_b + \tau_s}{\frac{a^2}{4R_{eff}^2} + \frac{\tau_s}{\tau_{2D}}} \quad (7)$$

where R_{eff} is the effective radius of the nanocavity (*i.e.* the radius of a sphere with the same volume as the nanocavity), $a = d_{eff}/2$, and $\tau_b = \tau_{3D}a^2/(4R_{eff}^2)$ is the characteristic time after which, a particle starting at a bounding plane, returns back to the plane (eqn (18) of Oshanin *et al.*[6]), and τ_s the typical time that a particle is trapped at the solid wall. For $\tau_s \to 0$, the particle is not trapped at the wall (which corresponds to our repul-

sive case), and eqn (7) gives $\tau \to \tau_{3D}$. In the opposite limit, $\tau_s \to \infty$, eqn (7) gives $\tau = \tau_{2D}$, *i.e.* if the trapping time τ_s is very large, the particle undergoes a 2D diffusion along the nanocavity wall. In our system, an estimation for τ_s comes from a Kramers-like approach and reads

$$\tau_s = \frac{1}{D}\int_{2^{1/6}\sigma_{LJ}}^{4\sigma_{LJ}} \exp[U(y)]\mathrm{d}y \int_0^x \exp[-\beta U(x)]\mathrm{d}x \qquad (8)$$

where U is the LJ potential reported in eqn (2) (see ESI Note S2†). The range of the first integral assumes that the particles starts from the minimum of the LJ-potential well ($x_0 = 2^{(1/6)}\sigma_{LJ}$, *i.e.* the most probable position) and escape when at a distance $4\sigma_{LJ}$ in the bulk. Only minor quantitative changes are observed if the upper bound is changed to other reasonable values (such as $3\sigma_{LJ}$). The integration can be easily numerically performed and τ_s as a function of ε is reported in Fig. 3a. Fig. 3b, in contrast, reports τ from eqn (8) for d_c = 400 nm and various d_{eff} ranging from 5 nm to 35 nm. In all cases, the curves resemble the scenario we observed in our Brownian simulations of Fig. 1b and S4.† For $\varepsilon < k_BT$, τ is almost constant, but then decreases in the interval $k_BT < \varepsilon < 5k_BT$, and then, for $\varepsilon \gtrsim 5k_BT$ a plateau (corresponding to the τ_{2D} value) is reached. The inset reports the quantitative comparison with numerical data showing a nice agreement, at least in the light of the large number of approximation needed to obtain eqn (7).

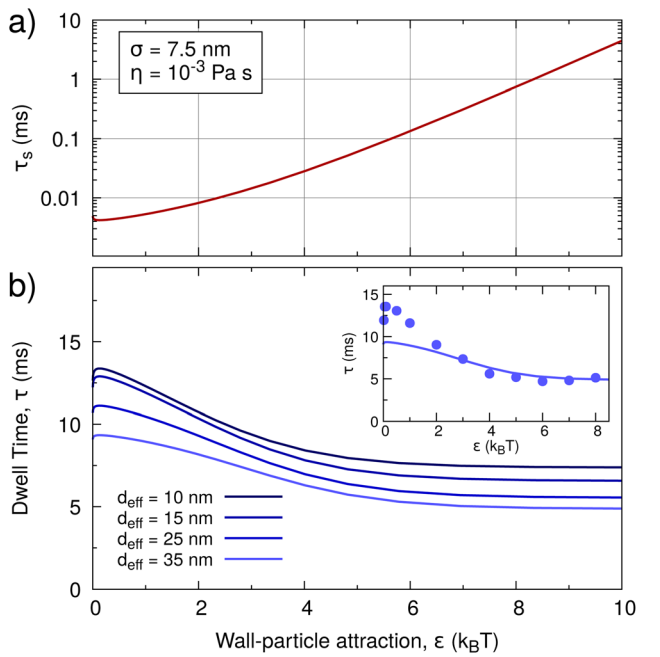

Fig. 3 2D–3D transition. (a) Escape time τ_s from a planar wall as a function of the wall–particle interaction as predicted by eqn (8) for σ_{LJ} = 7.5 nm, with all other parameters identical to those in Fig. 1. (b) Dwell time τ from eqn (7) for d_c = 400 nm and d_{eff} = 10, 15, 25, 35 nm. The inset reports comparison with numerical data for d_c = 400 nm and d_{eff} = 35 nm already shown in Fig. 1.

3.2 Effect of mobility reduction

Finally, we incorporate the effects of drag resulting from proximity to the nanocavity wall as a reduction in the mobility coefficient. More specifically, in eqn (3) we set the mobility at the wall to $\mu_w = f\mu_b$ with μ_b the bulk mobility and $f < 1$. In essence, when the particle is trapped at the wall (*i.e.* it is in the area of the attractive well of the LJ potential), and μ is reduced by a factor f. The smoothing between the bulk value μ_b and the wall value μ_w is the sigmoid curve provided in eqn (3) and sketched Fig. 4a. The change in the particle mobility at the wall may arise from several phenomena. For instance, in the event of repulsive particle–wall interactions, we expect that the main contribution will came from hydrodynamics. In this case, one can rely on approximated expressions for mobility of a particle near a wall[51] or on numerical approaches[43] if the

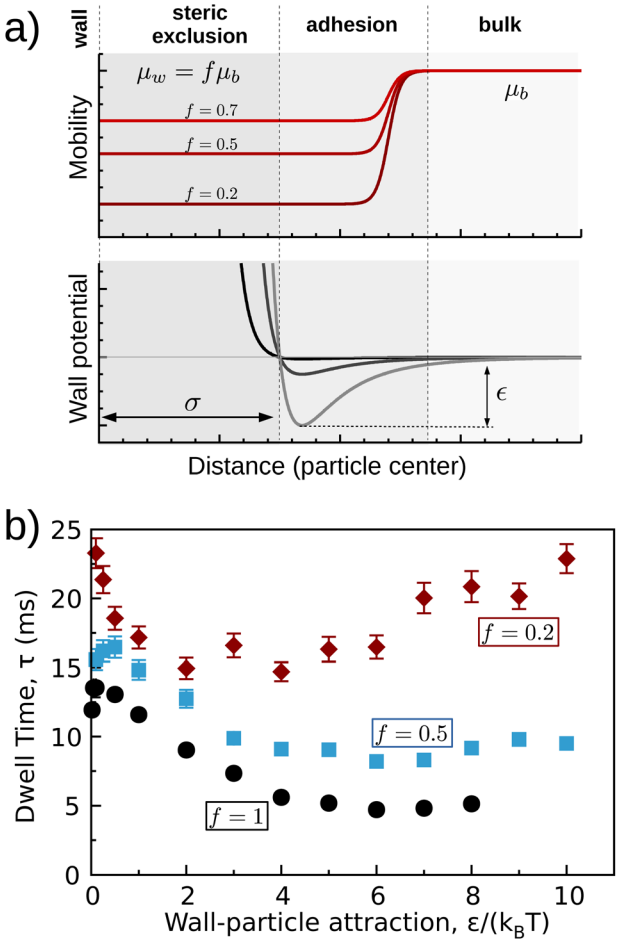

Fig. 4 Effect of reduction of the wall mobility. (a) The mobility of the particle is modeled as a sigmoid (eqn (3)). Far from the wall, the mobility has the bulk value μ_b, while close to the wall, when the particle is trapped in the well of the potential representing the wall–particle interaction, the mobility is reduced by a factor f, *i.e.* $\mu_w = f\mu_b$. (b) Average dwell time τ as a function of intensity ε of the wall–particle interaction for f = 0.2 and f = 0.5 for d_c = 400 nm and d_e = 50 nm. For comparison, the case with no mobility reduction (already presented in Fig. 1) is also reported.

liquid slippage may strongly alter the dynamics close to a wall (as it happens in a wide range of transport phenomena[52,53]). For highly attractive walls, we may instead expect that the main source of mobility reduction will be the partial adsorption due to chemical affinity. In nanopore sensing applications, another possibility is that the coating of a solid-state pore with a fluid-like membrane able to bind the particle.[54,55]

When mobility at the wall is reduced, the dependence of the dwell time on the depth ε of the wall–particle interaction is no longer monotonic (see Fig. 4b). Indeed, now the reduction in the dwell time due to the surface diffusion is compensated for by the increase in the drag. For the highly attractive case ($\varepsilon \geq 8k_BT$), the dwell time τ tends to a plateau for all three curves in Fig. 4b. As expected from the theoretical expression for the dwell time for the 2D surface diffusion (eqn (5)), τ scales to roughly as $1/f$ (for instance, the plateau value for $f = 0.5$ is approximately the double of the plateau value for $f = 1$). Interestingly, for low f (*i.e.* the mobility is largely reduced at the wall) the dwell time shows a minimum for intermediate values of ε (see red points in Fig. 4b). An additional phenomenon of note is the effect of a change in the value of σ_μ on the dwell time of an analyte within a confined volume. As can be seen in ESI Fig. S5,† when all other factors are constant, an increase in σ_μ (which roughly correlates to an ever-greater distance from the wall where mobility reduction becomes measurable) results in an increase in the average dwell time τ. While this effect is somewhat limited for the repulsive case (likely due to the fact that the particle in not trapped in the wall region where the mobility is reduced), it is much more pronounced for the attractive wall case. As expected, in both repulsive and attractive case, when σ_μ approach to the particle size $d_p/2$ the dwell time is comparable to that of an identical scenario with no mobility reduction.

4 Conclusions

In this study, we employed Brownian simulations to simulate the exit of a particle from a nanocavity. The Brownian model has computational cost much lower compared with other coarse grained approaches and is able to include thermal fluctuation such as DPD[56–60] or MPCD.[61,62] This allowed us to explore the effects of a wide range of parameters on particle trajectories within a confined volume. In particular, we investigated the effects on the average dwell time of particle–wall interactions, as well those of the size of the nanocavity and of the aperture, as well as that of a reduction in particle mobility when the analyte adheres the wall.

Varying the intensity of particle–wall attractive interaction had an intriguing effect on the dwell time. For repulsive walls, the particles explored the nanocavity volume until they reach one of the apertures. For sufficiently attractive particle–wall interactions, on the other hand, becomes trapped upon contact with the wall starts diffusing along the nanocavity surface. This 2D diffusive process allows the particle to escape more quickly. Overall, the dwell time of the particle decreases with the strength of the wall–particle interaction until a plateau is reached for interaction energies with minima's less than $\sim 5k_BT$. Since exact theoretical results in the literature were found only for more ideal geometries (such as spheres or disks), our simulation may be used to test the capability of existing theoretical models for more complex system geometries which have a greater similarity to some laboratory conditions. The comparison with existing theories indicates that analytical models are able to predict the trends of the dwell time as a function of the nanocavity and aperture size in the 2D and the 3D case and even to catch some features of the 2D–3D transition. Our simulation also allowed us to study the effect of the reduction of the mobility at the wall. If the wall mobility is much lower than that of the bulk, the 2D scenario is no longer the faster way for the particle to leave the nanocavity. Taken together, we think that our results may contribute to the understanding of how geometry and wall–particle interactions may be tuned to control the dwell time of a particle within a confined space. From a practical perspective, once estimations on the reduction of mobility at the wall and on the intensity of the particle–wall interaction are available, this information may be embedded in the Brownian solver. This evidence may come from experiments[63–65] or, alternatively, from atomistic simulations.[66]

However, as the experimental data for pure volumetric confinement (the focus of our work) is extremely limited, we have found it necessary to design our own novel, *in situ* experimental methodology. This will form the basis of future work into refining our model to more closely match laboratory conditions. Overall, the understanding of the escape time from a nanocavity may be relevant in developing nanopore–nanocavity systems for sensing single particles or to monitor the interaction of a small number of molecules.

Conflicts of interest

There are no conflicts of interest to declare.

Notes and references

1 D. Holcman and Z. Schuss, *Rep. Prog. Phys.*, 2013, **76**, 074601.
2 D. Holcman, N. Hoze and Z. Schuss, *Phys. Rev. E: Stat., Nonlinear, Soft Matter Phys.*, 2011, **84**, 021906.
3 Z. Schuss, A. Singer and D. Holcman, *Proc. Natl. Acad. Sci. U. S. A.*, 2007, **104**, 16098–16103.
4 O. Bénichou and R. Voituriez, *Phys. Rep.*, 2014, **539**, 225–284.
5 D. S. Grebenkov and G. Oshanin, *Phys. Chem. Chem. Phys.*, 2017, **19**, 2723–2739.
6 G. Oshanin, M. Tamm and O. Vasilyev, *J. Chem. Phys.*, 2010, **132**, 06B607.
7 O. Bénichou, D. Grebenkov, P. Levitz, C. Loverdo and R. Voituriez, *Phys. Rev. Lett.*, 2010, **105**, 150606.

8 D. Holcman and Z. Schuss, *J. Stat. Phys.*, 2004, **117**, 975–1014.
9 S. Zeng, M. Chinappi, F. Cecconi, T. Odijk and Z. Zhang, *Nanoscale*, 2022, **14**, 12038–12047.
10 D. Pedone, M. Langecker, G. Abstreiter and U. Rant, *Nano Lett.*, 2011, **11**, 1561–1567.
11 E. L. Bonome, F. Cecconi and M. Chinappi, *Nanoscale*, 2019, **11**, 9920–9930.
12 F. Bétermier, B. Cressiot, G. Di Muccio, N. Jarroux, L. Bacri, B. Morozzo della Rocca, M. Chinappi, J. Pelta and J.-M. Tarascon, *Commun. Mater.*, 2020, **1**, 59.
13 Y. N. D. Bandara, N. Farajpour and K. J. Freedman, *J. Am. Chem. Soc.*, 2022, **144**, 3063–3073.
14 N. Meyer, I. Abrao-Nemeir, J.-M. Janot, J. Torrent, M. Lepoitevin and S. Balme, *Adv. Colloid Interface Sci.*, 2021, **298**, 102561.
15 I. M. F. Tanimoto, B. Cressiot, N. Jarroux, J. Roman, G. Patriarche, B. Le Pioufle, J. Pelta and L. Bacri, *Biosens. Bioelectron.*, 2021, **183**, 113195.
16 F. Farhangdoust, F. Cheng, W. Liang, Y. Liu and M. Wanunu, *Adv. Mater.*, 2022, **34**, 2108479.
17 X. Liu, M. M. Skanata and D. Stein, *Nat. Commun.*, 2015, **6**, 6222.
18 Y. Zhang, X. Liu, Y. Zhao, J.-K. Yu, W. Reisner and W. B. Dunbar, *Small*, 2018, **14**, 1801890.
19 F. A. Morrison Jr., *J. Colloid Interface Sci.*, 1970, **34**, 210–214.
20 M. Boukhet, F. Piguet, H. Ouldali, M. Pastoriza-Gallego, J. Pelta and A. Oukhaled, *Nanoscale*, 2016, **8**, 18352–18359.
21 S. Tanaka, M. Tsutsui, H. Theodore, H. Yuhui, A. Arima, T. Tsuji, K. Doi, S. Kawano, M. Taniguchi and T. Kawai, *Sci. Rep.*, 2016, **6**, 31670.
22 L. Liu, K. Chen, N. Xiang and Z. Ni, *Electrophoresis*, 2019, **40**, 873–889.
23 C. Liao, F. Antaw, A. Wuethrich and M. Trau, *Adv. Mater. Technol.*, 2020, **5**, 2000701.
24 N. H. Pham, Y. Yao, C. Wen, S. Li, S. Zeng, T. Nyberg, T. T. Tran, D. Primetzhofer, Z. Zhang, S.-L. Zhang, *et al.*, *ACS Nano*, 2021, **15**, 17938–17946.
25 J. P. Fried, J. L. Swett, B. P. Nadappuram, J. A. Mol, J. B. Edel, A. P. Ivanov and J. R. Yates, *Chem. Soc. Rev.*, 2021, **50**, 4974–4992.
26 S. Zeng, C. Wen, S. Li, X. Chen, S. Chen, S.-L. Zhang and Z. Zhang, *Nanotechnology*, 2019, **30**, 455303.
27 S. Li, S. Zeng, C. Wen, L. Barbe, M. Tenje, Z. Zhang, K. Hjort and S.-L. Zhang, *J. Phys. Chem. B*, 2020, **124**, 11573–11583.
28 L. Qiao and G. W. Slater, *Phys. Chem. Chem. Phys.*, 2022, **24**, 6444–6452.
29 T. Y. Molotilin, V. Lobaskin and O. I. Vinogradova, *J. Chem. Phys.*, 2016, **145**, 244704.
30 C. C. Wells, D. V. Melnikov and M. E. Gracheva, *J. Chem. Phys.*, 2019, **150**, 115103.
31 G. A. Huber and J. A. McCammon, *Trends Chem.*, 2019, **1**, 727–738.
32 C. Y. Kong and M. Muthukumar, *Electrophoresis*, 2002, **23**, 2697–2703.
33 P. Lançon, G. Batrouni, L. Lobry and N. Ostrowsky, *Europhys. Lett.*, 2001, **54**, 28.
34 M. S. Miguel and R. Toral, *Instabilities and nonequilibrium structures VI*, Springer, 2000, pp. 35–127.
35 N. G. van Kampen, *Stochastic processes in physics and Chemistry*, North-Holland, 2008.
36 T. Schlick, *Molecular modeling and simulation: An interdisciplinary: Guide*, Springer, 2014.
37 S. Tan, L. Wang, H. Liu, H. Wu and Q. Liu, *Nanoscale Res. Lett.*, 2016, **11**, 1–10.
38 E. M. Purcell, *Am. J. Phys.*, 1977, **45**, 3–11.
39 S. Kim and S. J. Karrila, *Microhydrodynamics: Principles and selected applications*, Butterworth-Heinemann, 1991.
40 T. M. Squires and S. R. Quake, *Rev. Mod. Phys.*, 2005, **77**, 977–1026.
41 I. V. Grigoriev, Y. A. Makhnovskii, A. M. Berezhkovskii and V. Y. Zitserman, *J. Chem. Phys.*, 2002, **116**, 9574–9577.
42 M. Lisicki, B. Cichocki and E. Wajnryb, *J. Chem. Phys.*, 2016, **145**, 034904.
43 D. Pimponi, M. Chinappi, P. Gualtieri and C. M. Casciola, *Microfluid. Nanofluid.*, 2014, **16**, 571–585.
44 T. Ala-Nissila, R. Ferrando and S. Ying, *Adv. Phys.*, 2002, **51**, 949–1078.
45 D. L. Ermak and J. McCammon, *J. Chem. Phys.*, 1978, **69**, 1352–1360.
46 A. Gubbiotti, M. Chinappi and C. M. Casciola, *Phys. Rev. E*, 2019, **100**, 053307.
47 A. W. Lau and T. C. Lubensky, *Phys. Rev. E: Stat., Nonlinear, Soft Matter Phys.*, 2007, **76**, 011123.
48 M. Chinappi, M. Yamaji, R. Kawano and F. Cecconi, *ACS Nano*, 2020, **14**, 15816–15828.
49 C. T. A. Wong and M. Muthukumar, *J. Chem. Phys.*, 2007, **126**, 164903.
50 A. Y. Grosberg and Y. Rabin, *J. Chem. Phys.*, 2010, **133**, 10B617.
51 A. J. Goldman, R. G. Cox and H. Brenner, *Chem. Eng. Sci.*, 1967, **22**, 637–651.
52 M. Manghi, J. Palmeri, K. Yazda, F. Henn and V. Jourdain, *Phys. Rev. E*, 2018, **98**, 012605.
53 E. S. Asmolov, A. V. Belyaev and O. I. Vinogradova, *Phys. Rev. E: Stat., Nonlinear, Soft Matter Phys.*, 2011, **84**, 026330.
54 E. C. Yusko, J. M. Johnson, S. Majd, P. Prangkio, R. C. Rollings, J. Li, J. Yang and M. Mayer, *Nat. Nanotechnol.*, 2011, **6**, 253–260.
55 O. M. Eggenberger, C. Ying and M. Mayer, *Nanoscale*, 2019, **11**, 19636–19657.
56 P. Espanol and P. Warren, *Europhys. Lett.*, 1995, **30**, 191.
57 P. Español and P. B. Warren, *J. Chem. Phys.*, 2017, **146**, 150901.
58 A. Gubbiotti, M. Chinappi and C. M. Casciola, *Eur. Phys. J. Plus*, 2022, **137**, 1–21.

59 D. S. Bolintineanu, G. S. Grest, J. B. Lechman, F. Pierce, S. J. Plimpton and P. R. Schunk, *Comput. Part. Mech.*, 2014, **1**, 321–356.
60 I. Pagonabarraga and D. Frenkel, *J. Chem. Phys.*, 2001, **115**, 5015–5026.
61 A. Malevanets and R. Kapral, *J. Chem. Phys.*, 1999, **110**, 8605–8613.
62 G. Gompper, T. Ihle, D. Kroll and R. Winkler, *Advanced computer simulation approaches for soft matter sciences III*, 2009, pp. 1–87.
63 V. Michailidou, G. Petekidis, J. Swan and J. Brady, *Phys. Rev. Lett.*, 2009, **102**, 068302.
64 P. Holmqvist, J. K. Dhont and P. R. Lang, *Phys. Rev. E: Stat., Nonlinear, Soft Matter Phys.*, 2006, **74**, 021402.
65 M. Matse, M. V. Chubynsky and J. Bechhoefer, *Phys. Rev. E*, 2017, **96**, 042604.
66 A. Baer, P. Malgaretti, M. Kaspereit, J. Harting and A.-S. Smith, *J. Mol. Liq.*, 2022, **368**, 120636.